Journal of Nuclear Materials 545 (2021) 152651

Contents lists available at ScienceDirect

Journal of Nuclear Materials

journal homepage: www.elsevier.com/locate/jnucmat

Benefit or harm of accident tolerant coatings on the low-cycle fatigue properties of Zr-4 cladding alloy: in-situ studies at 400°C

Xianfeng Ma, Hailin Zhai, Fanqiang Meng, Jishen Jiang*, Xiujie He, Yanying Hu, Wenjie Zhang, Jiajun Tu, Donghui Wei, Biao Wang

Sino-French Institute of Nuclear Engineering and Technology, Sun Yat-Sen University, Zhuhai 519082, Guangdong, China

ARTICLE INFO

Article history:
Received 18 June 2020
Revised 23 September 2020
Accepted 30 October 2020
Available online 6 November 2020

Keywords:
Accident tolerant coating
Cr
TiCrAlN
Zr-4 alloy
Low cycle fatigue
In-situ SEM

ABSTRACT

The present work is the first study investigating the effects of accident tolerant coatings on the low-cycle fatigue life of the Zr-4 alloy. Zr-4 alloy with different accident tolerant coatings, i.e., a Cr coating or a TiCrAlN coating by multi-arc ion plating, were studied at 400°C by in-situ fatigue testing with a scanning electron microscope (SEM). It was surprisingly found that the Cr coating improved the fatigue life of the Zr-4 alloy significantly, whereas the TiCrAlN coating decreased the fatigue life dramatically. The fatigue life variation was closely related to the ratcheting strain of each type of sample in this study. Further, in-situ SEM observations indicated that the Cr coating exhibited a good capacity for plastic deformation with the Zr-4 substrate until the late stage of fatigue life. In contrast, for the TiCrAlN coating, multiple cracks formed during the early stage of fatigue life. The distinct effects of the two coatings were confirmed by analysis of the fracture surfaces and longitudinal section microstructure. Hence, variations in the fatigue life of the coated Zr-4 samples was attributed to the cyclic deformation and cracking behavior of each coating. Finite element simulations based on the cohesive element method indicated that the pre-failure of the brittle TiCrAlN coating (with its low fracture toughness) promoted early crack initiation in the Zr-4 substrate, leading to a short fatigue life. For the Cr coating (with its high fracture toughness and good plasticity), the crack initiation in the substrate was postponed, leading to a longer fatigue life.

1. Introduction

Zirconium alloys have been widely used as nuclear fuel cladding materials in light water reactors (LWRs) for decades because of their low neutron capture cross section, excellent corrosion resistance, and thermo-mechanical properties [1]. However, under a loss of coolant accident (LOCA) condition, the reaction of Zr alloys with steam at high temperatures may result in hydrogen uptake, which greatly threatens the nuclear safety of LWRs. Since the Fukushima accident in Japan, the development of accident tolerant fuel (ATF) has attracted increasing interest from researchers in the field of nuclear safety and nuclear fuels [2]. Among the different ATF strategies, applying a surface coating on the Zr-4 cladding alloy has been regarded as a favorable candidate [3]. Coatings with superior oxidation resistance would be specially fabricated on the surface of the cladding to prevent the contact and reaction with hot steam. One major benefit of the ATF coating strategy is the convenience of application because it does not alter the structure of the claddings nor disrupt the design and manufacture of the nuclear fuel system.

In recent years, progress has been made in the material selection and fabrication technology of ATF coatings on Zr alloys [3]. The coatings reported in the literature include ceramic coatings (MAX phase [4], SiC [5], ZrC [6], and TiCrAlN [7]), metallic coatings (Cr [8] and FeCrAl [9]), and multilayer composite coatings (Cr-Zr/Cr/CrN [10] and ZrO_2/FeCrAl [11]). Ma et al. [7] evaluated the corrosion and oxidation behaviors of the TiAlCrN ceramic coatings prepared by the multi-arc ion plating technique. The coated samples showed minimal weight gain and no obvious coating spallation after a corrosion test in pure water at 360°C and 18.5 MPa, nor after a high temperature oxidation test at 1060°C in air. Alat et al. [12] found that the weight gain of the multilayer TiN-TiAlN ceramic-coated Zircaloy was six times lower than that of the uncoated samples, and the coating adhered well to the substrate after a corrosion test at 360°C and 18.7 MPa for 90 days. In addition, Cr-based coatings have been considered to have many possible applications because of their superior oxidation resistance, high melting point, and similar thermo-mechanical proprieties to the substrate Zr alloy. Kim et al. [13] prepared a Cr coating on a Zr-based alloy using the 3D laser coating method and found that the

* Corresponding author.
E-mail address: Jiangjsh3@mail.sysu.edu.cn (J. Jiang).

https://doi.org/10.1016/j.jnucmat.2020.152651
0022-3115/

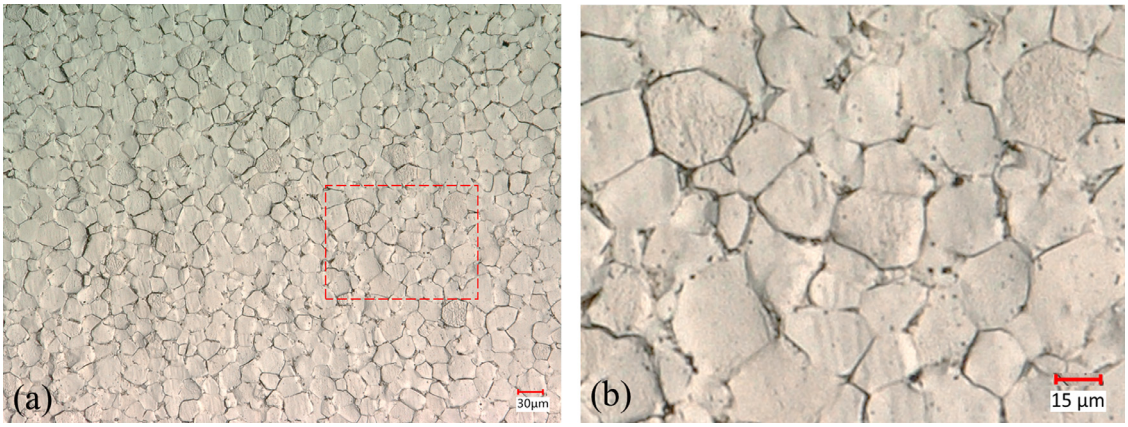

Fig. 1. Microstructure of the annealed Zr-4 alloy: (a) optical image, (b) high magnification of (a).

thickness of the oxide layer on the Cr-coated surface was ~25 times lower than that of the uncoated surface. Brachet et al. [14] assessed the corrosion, oxidation resistance, and mechanical properties of the Cr-coated nuclear cladding in LOCA and beyond LOCA conditions. They found that the Cr coating/Zr substrate system not only had good corrosion and oxidation resistance but also high tensile strength, wear resistance, and interfacial adhesion.

While the corrosion and oxidation resistance of several ATF coatings have been extensively studied, there is little information available on the strength assessment and failure mechanisms of the ATF coatings at high temperatures. During the operation of the reactors, the fuel cladding generally undergoes cyclic thermal and mechanical loading conditions from the combination of the flow vibration of the water cooling medium and temperature changes caused by the core power adjustment [15]. Therefore, knowledge about the effect of ATF coatings on the mechanical properties (e.g., low-cycle fatigue (LCF) life) of Zr alloy cladding at high temperatures is an essential performance index that must be studied before the application of a coating candidate.

It is known from previous research that ceramic and metallic coatings may remarkably affect the fatigue lives of the coated bodies [16]. Lonyuk et al. [17] found that the fatigue life of NiP-coated aluminum alloys was 50% longer than that of uncoated samples, which benefited not only from the higher strength of the coating compared to the substrate but also from the compressive residual stress in the coating from the deposition process. However, Lonyuk et al. [18] found that the 60 μm thick oxide coatings led to ~75% reduction in the fatigue strength of the 7475-T6 aluminum alloy, which was primarily associated with the stress concentration at the micro-cracks in the coatings. Similar phenomenon were also found in some brittle coatings [19,20]. Various factors, such as the ratio of the coating/substrate strength and interfacial adhesion, as well as the residual stress and microstructure of the coating, can affect the fatigue properties of the coated substrate [17]. Reviewing the ATF coating candidates with superior oxidation and corrosion resistance, there are ceramic coatings with high hardness and metallic coatings with excellent ductility. For different coatings, the mechanisms that influence the fatigue life might be distinct. Hence, it is critical to clarify how and why ATF coatings affect the fatigue properties of Zr alloys.

For this purpose, the present study attempts to explore the effects of two ATF coatings, i.e., a Cr coating and a TiCrAlN coating, on the LCF life of the Zr-4 alloy at 400°C. In-situ scanning electron microscope (SEM) fatigue tests were conducted at 400°C to understand the deformation and fracture mechanism of different samples. Three groups of samples, namely, uncoated, Cr-coated, and TiCrAlN-coated Zr-4 samples, were prepared and tested. Comparative studies of the LCF properties, deformation mechanism, and crack evolution in different samples were carried out.

2. Materials and experimental

2.1. Materials

The chemical composition of the Zr-4 alloy used in this study is given in Table 1. The as-received Zr-4 rod had a diameter of 25 mm, which was subjected to an annealing heat treatment at 800°C for 24 h in a vacuum. The microstructure of the annealed Zr-4 alloy is shown in Fig. 1. The average grain size of the Zr-4 alloy was about 20 μm. Subsequently, the Zr-4 alloy was machined into fatigue samples following the geometry shown in Fig. 2. The fatigue samples were ground by 360, 600, 800, 1000, and 1200 grit SiC papers to remove the surface oxide film and to achieve the optimum surface asperity for coating adhesion. The thicknesses of the test samples ranged from 0.50 to 0.65 mm due to different polishing losses. After grinding, the samples were cleaned by the following procedure: 1) exposed to ethyl alcohol for 10 min in an ultrasonic cleaner; 2) rinsed with deionized water; and 3) dried with nitrogen gas.

The Cr and TiCrAlN coatings were deposited on the Zr-4 alloy substrate by the multi-arc ion plating technique. A hole 1.5 mm in diameter was drilled into the region adjacent to one edge of the substrate for hanging during deposition. The samples hung on

Table 1
Chemical composition of the Zr4 alloy substrate.

	Sn	Fe	Cr	N	O	H	Zr
wt%	1.2-1.7	0.18-0.24	0.07-0.13	0.008	0.16	0.01	Bal.

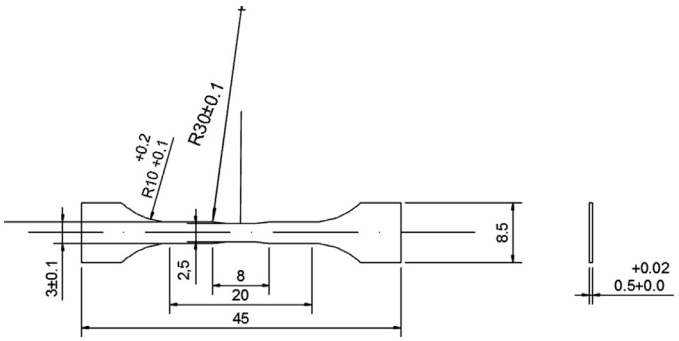

Fig. 2. Geometry of fatigue specimen (all dimensions in mm).

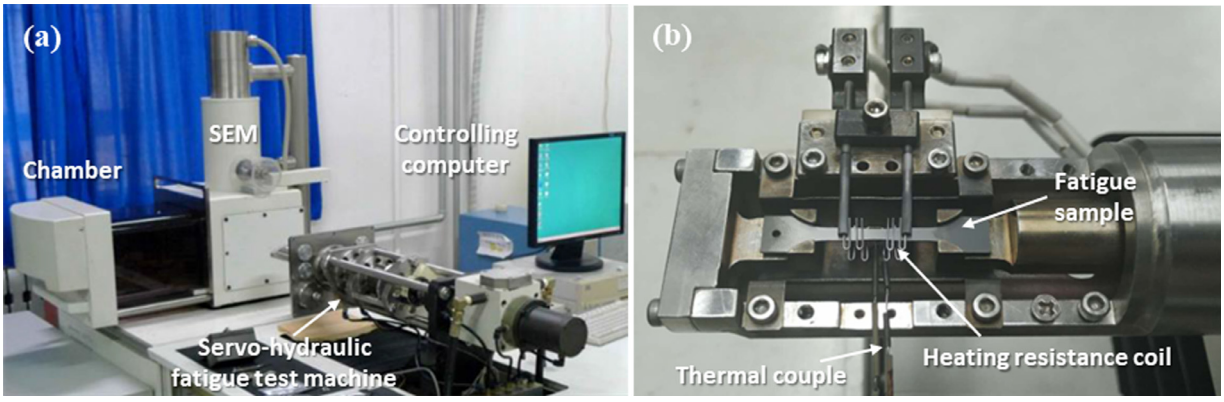

Fig. 3. In-situ fatigue testing system with an SEM for elevated temperature testing: (a) SEM and control system, and (b) fatigue sample loading unit.

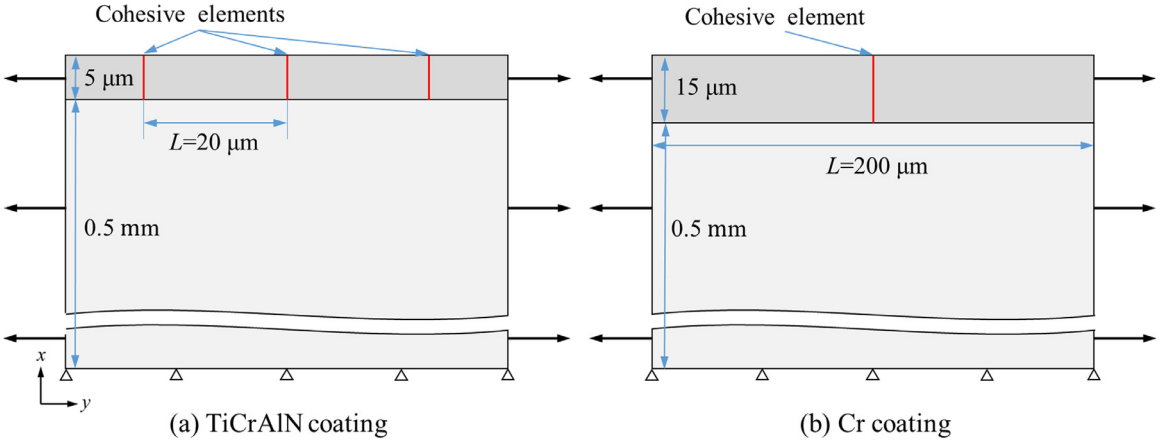

Fig. 4. FE models of the (a) TiCrAlN-coated and (b) Cr-coated Zr-4 alloys.

the holder and rotated at a constant speed to obtain homogenous deposited coatings. Before deposition, sputter cleaning was performed on the samples at a bias potential of 500 V to remove the oxide from the substrate surface. The Cr coatings were deposited using two high-purity (99.999%) Cr cathodes under a negative substrate bias voltage of 75 V, an arc current of 100 A, a pressure of 2.7 Pa, a deposition temperature of 340°C, and a deposition time of 8 h. To prepare the TiCrAlN coatings, a Cr bond coating approximately 100 nm thick was first deposited on the Zr-4 substrate under an argon atmosphere at a pressure of 0.3 Pa to enhance the interfacial adhesion. Two high-purity (99.999%) Cr cathodes and two TiAl (25-75 at.% Al) cathodes were used for the deposition of TiCrAlN layers under a negative substrate bias voltage of 70 V, an arc current of 100 A, a pressure of 0.3 Pa, and a deposition time of 3 h. The temperature of the substrates was maintained at 400°C during deposition, and the nitrogen and argon flows were kept at 200 ml/min and 30 ml/min, respectively.

2.2. Experimental procedure

As shown in Fig. 3, the LCF tests of all samples were performed at 400°C in the vacuum chamber of an SEM using a specially designed servo-hydraulic testing system. The elevated temperature was achieved by heating resistance coils, accompanied with a thermocouple to obtain a stable temperature. The sample was first heated to 400°C and then held for 15 min before each fatigue test. The fatigue tests were performed under a controlled load using a sinusoidal waveform with a stress ratio of R = 0.1 and a loading frequency of 10 Hz. During testing, the evolution of the engineering strain parallel to the loading direction was obtained by measuring the variation of the displacement of the gauge section. The tests were paused at different required loading cycles and held at average stress to capture the micro-cracking and microstructure evolution of the fatigue samples under the secondary electron mode of the SEM. Note that since the times for taking SEM images were short and the temperature was relatively low, the creep effect on the fatigue testing was negligible. All the coated and uncoated samples were tested to failure. After fatigue testing, each fatigue sample was subjected to fractography analyses in the SEM (TESCAN MIRA 3, Czech). In addition, some samples of the Zr-4 alloys with a Cr or TiCrAlN coating were cut at the gage section to obtain the longitudinal section microstructures, which can reveal the fatigue crack morphology.

3. Finite element modeling

To understand the evolution of surface cracks in both the TiCrAlN coating and the Cr coating during the fatigue test, two-dimensional plane strain finite element (FE) models were built. Fig. 4 shows the geometry of the FE models of the TiCrAlN and Cr coating systems. The coatings and the Zr-4 substrate for both models are assumed to bond together tightly without any interfacial cracks, and the interfaces are assumed to be flat. Based on the experimental measurement, the thicknesses of the TiCrAlN coating, Cr coating and substrate are set as 5 μm, 15 μm and 0.5 mm, respectively. Four-node plain strain elements are adopted to mesh the coatings and the substrates in both models, and the meshes in regions near the interfaces and the vertical cracks are refined to enhance the calculation accuracy. To model the vertical surface cracks, four-node cohesive elements (COH2D4) in zero thicknesses

Table 2
Mechanical properties of the TiCrAlN coating, Cr coating, and Zr-4 substrate at 400°C.

	E (GPa)	v	σ_s (MPa)	σ_b (MPa)	Ref.
TiCrAlN coating	351	0.1	/	/	[19]
Cr coating	168	0.22	165	/	[23,24]
Zr-4 substrate	71	0.32	135.5	210	[22]

are inserted vertically in the coatings, as shown in Fig. 4. Vertical cracks are restricted to initiate and propagate along the cohesive elements under deformation. During fatigue tests, the surfaces cracks on both coatings continuously grow and finally reach a plateau stage, namely the crack densities reach saturation, under large deformation. Thus, the distances between two adjacent vertical cracks, L, are set to be 20 μm and 200 μm for the TiCrAlN coating and Cr coating, respectively, which are equal to the average values of the saturated cracks for both coatings. In Fig. 4, considering the periodic geometries of the models, a three-period model for the TiCrAlN coating system and a one-period model for the Cr coatings system are built for FE calculation. In the two models, the left and right edges are imposed the periodical boundary conditions by the multi-point constraint (MPC) method [21]. The bottom edges of the substrates are restricted to move in the y direction, while the top edges of the coatings are free from any constraint.

Instead of fatigue load, uniform linear tensile loads at 400°C were applied on the two FE models to simplify the calculations. The models assume that initiation and propagation of the vertical cracks are primarily related to the continuous increase in the ratcheting strain during fatigue tests, and the effects of variations in the fatigue loadings were not taken into account. Despite the simplification, the stress evolution and vertical cracking in the two coatings can be compared, and an explanation for the difference in fatigue cracking between the coatings can be provided based on the FE results.

The ceramic TiCrAlN coatings are regarded as the elastic material, while the Cr coating and the Zr-4 substrate are regarded as elastic-plastic materials [22-24]. Since no mechanical properties of the TiCrAlN coating are available, its elastic properties are assumed to be similar to those of the ceramic CrAlN coating [19]. The mechanical properties, such as the elastic modulus E, Poisson's ratio v, yield stress σ_s and ultimate tensile strength σ_b of all materials at 400 °C are listed in Table 2.

The constitutive relation of the cohesive elements for modeling vertical cracks can be described by a bilinear traction-separation law (TSL), which assumes that the cohesive element ahead of the crack tip has a linear elastic behavior before damage, once the damage criterion is satisfied, namely the stress reaches a critical value σ_b, damage will be initiated. Under continuous loadings, damage will be accumulated with a linear stress softening. Once the damage value reaches 1, the stress decreases to zero and final failure happens. At this moment, the related cohesive element will be deleted to represent a crack surface. Detailed descriptions of the cohesive zone model (CZM) and TSL could be found in our previous work [21,24]. In the bilinear TSL, six parameters, namely, the tensile strength σ_n^0, shear strength σ_s^0, initial stiffnesses K_n and K_s in normal and tangential directions (respectively), and critical energy release rates (i.e., the fracture toughness) G_{nc} and G_{sc} in normal and tangential directions (respectively), need to be defined [25]. However, because the TiCrAlN and Cr coatings are newly developed ATF coating systems in the last few years, the data of fracture parameters is lacking and thus rough assessments of these parameters are conducted. For the ceramic TiCrAlN coating, the tensile strength and fracture toughness are relatively lower, and vertical cracks appear early with the tensile strain of 2% based on the experimental results. The σ_n^0 and σ_s^0 were set to 50 MPa and G_{nc} and G_{sc} were set to 100 J/m^2 based on our multiple trial FE calculations. For the Cr coating at 400°C, the tensile strength was assumed to be equal to the ultimate tensile strength [23], and the fracture toughness ranged from 100 to 300 J/m^2 based on Ref. [26]. Thus, σ_n^0 and σ_s^0 were set to 210 MPa, and G_{nc} and G_{sc} were set to 200 J/m^2. For both coatings, K_n and K_s can be regarded as penalty parameters for the FE calculation, and their magnitudes have little effect on the crack modeling; therefore, appropriate values were set to avoid convergence problems. Despite the rough assumption on the fracture parameters, a comparative study on the stress evolution and cracking behavior in the two coatings can still be carried out. Efforts to evaluate the fracture parameters for the two coatings will be made in future work.

4. Results and discussion

4.1. Microstructure of the coatings

The surface morphology and cross-section microstructure of the as-prepared TiCrAlN- and Cr-coated samples are shown in Fig. 5. After deposition, the average thicknesses of the TiCrAlN and Cr coatings were 5.0 μm and 15.0 μm, respectively. Figs. 5(a) and 5(b) show the surfaces of the TiCrAlN and Cr coatings, in which some droplets with a diameter between 0.1 μm and 2 μm were inevitably formed. It is a common phenomenon reported in the coatings prepared by the arc ion plating technology [27], for which the size and morphology of the droplets are associated with the plating parameters, such as the gas pressure and bias potential [28]. As seen from the cross-sectional morphologies in Figs. 5(c) and 5(d), both the TiCrAlN and Cr coatings had dense microstructures and uniform thicknesses. The coatings and substrates were tightly bonded, and the interfaces were relatively flat. No micro-cracks were found either at the interface or on the surface.

4.2. Evaluation of the fatigue properties

The fatigue lives of the uncoated and coated Zr-4 samples at different stress levels at 400°C are listed in Table 3, and Fig. 6 shows the stress versus fatigue life curves (i.e., S-N curves) of the uncoated and coated Zr-4 samples. It is remarkable that the Cr coating can evidently improve the LCF life of the Zr-4 alloy, whereas the TiCrAlN coating remarkably deteriorates the fatigue life of the Zr-4 alloy, which has been rarely reported in previous studies of accident tolerant coatings. The improvement or deterioration of fatigue properties in the coated samples may be attributed to several factors, such as the strength and ductility of the coatings, interfacial adhesion between the coatings and substrates, and micro-crack evolution. Detailed analyses will be presented in the following sections.

In the present fatigue tests, the stress ratio of R = 0.1 was adopted. Under asymmetric stress-controlled cycling, inelastic deformation accumulation would be expected in the uncoated and coated Zr-4 alloys, i.e., the well-known ratcheting effect in the cycling process. Ratcheting behavior has been generally regarded to shorten the LCF life of alloys [22,29]. In previous studies of Zr alloys [22,30], evidence of ratcheting behavior was reported under a high average stress at high temperatures. In this work, the ratcheting strain ε_r is defined as follows:

$$\varepsilon_r = \frac{1}{2}(\varepsilon_{max} + \varepsilon_{\min}) \quad (1)$$

where $\varepsilon_{\max}$ and $\varepsilon_{\min}$ are the maximum and minimum strain of each cycle, respectively. Fig. 7 shows the ratcheting strain evolution for different samples. The applied loads are chosen inconsistent to present a clear and intuitive comparison between the coated and uncoated samples. Each ratcheting strain curve can be divided into

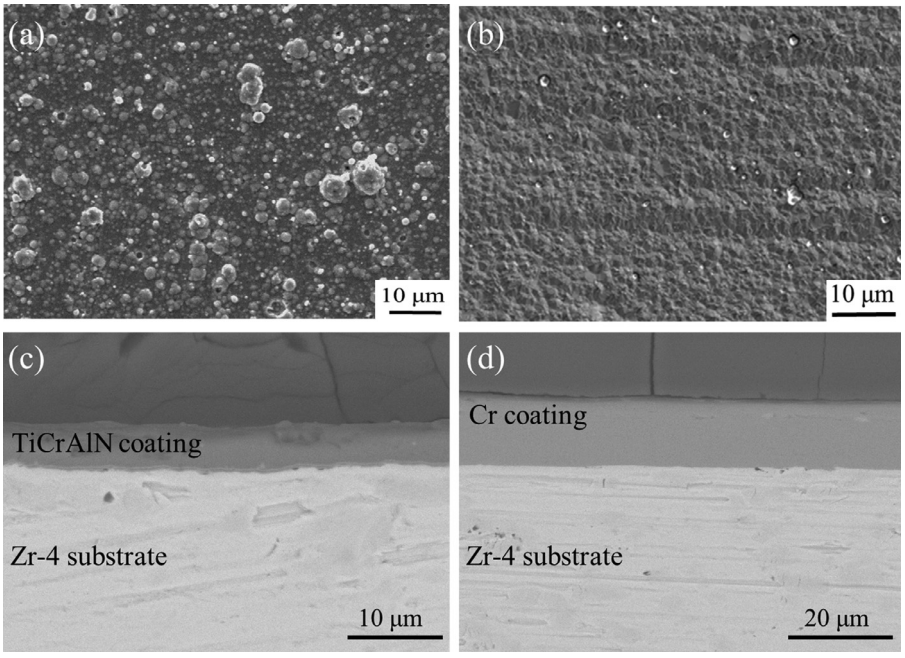

Fig. 5. Surface and cross-section morphologies of the TiCrAlN and Cr coated samples: (a) surface morphology of the TiCrAlN coating, (b) surface morphology of the Cr coating, (c) cross-section morphology of the TiCrAlN coating, and (d) cross-section morphology of the Cr coating.

Table 3
Fatigue lives of the uncoated and coated Zr-4 samples at different stress levels at 400°C.

Uncoated Zr-4		TiCrAlN coated Zr-4		Cr coated Zr-4	
Stress (MPa)	Fatigue life (-)	Stress (MPa)	Fatigue life (-)	Stress (MPa)	Fatigue life (-)
205	124504	190	36553	230	62180
215	19250	195	23995	238	12320
220	8680	210	4361	250	10440
225	21900	215	5560	255	1331
230	6010	220	1485	265	369
238	265				

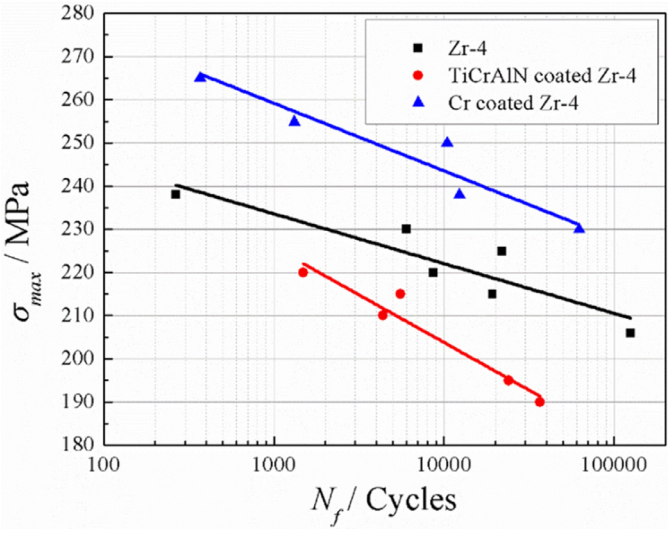

Fig. 6. Maximum stress vs. number of fatigue cycles (S-N curves) for uncoated, Cr-coated and TiCrAlN-coated Zr-4 alloys at 400 °C.

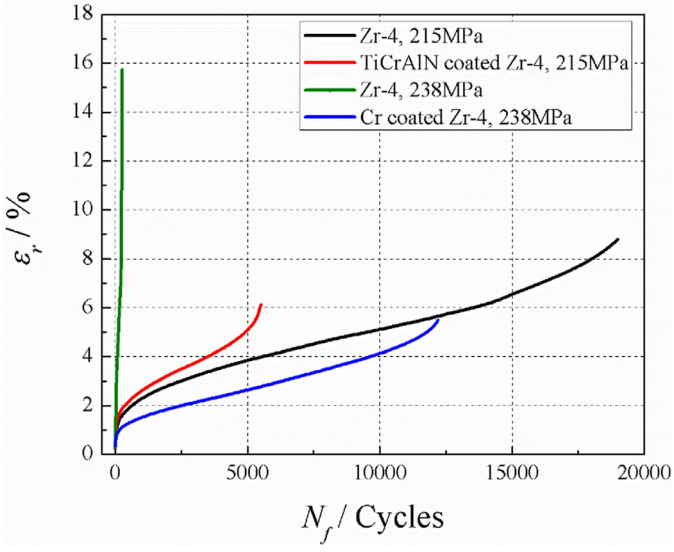

Fig. 7. Ratcheting strain curves of uncoated, Cr-coated, and TiCrAlN-coated Zr-4 alloys at 400°C.

three stages: the transient stage (stage I), steady stage (stage II), and tertiary stage (stage III). During stage I, the ratcheting strain increased rapidly with a decreasing strain rate, and it reached a steady increase state in a very short time. During stage II, the accumulation of ratcheting strain maintained an almost constant increasing rate for a long time. It is apparent that a higher stress level led to a more rapid strain increase. During the last stage, the strain accumulated at an accelerated rate and resulted in the

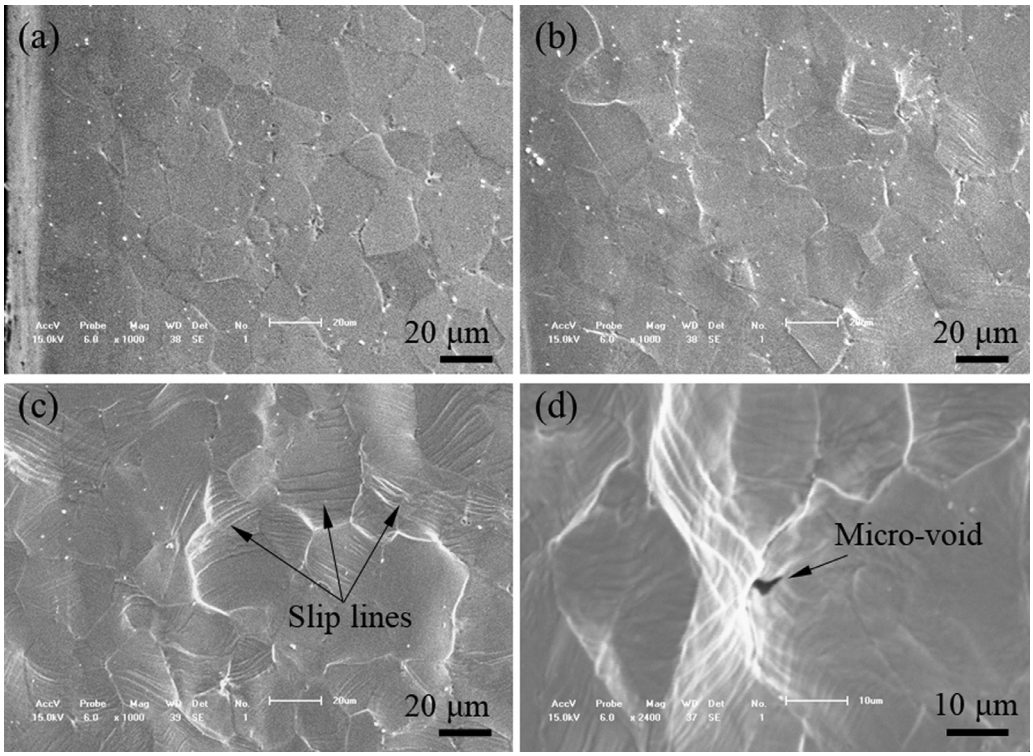

Fig. 8. In-situ observations of fatigue deformation in the uncoated Zr-4 alloy under 215 MPa at 400°C: (a) 0, (b) 1500, (c) 18100, and (d) 19210 cycles.

ultimate failure of the samples. As shown in Fig. 7, the TiCrAlN-coated sample had a more rapid increase in the ratcheting strain and reached the tertiary stage earlier than the uncoated sample at 215 MPa, while the Cr-coated sample had a slower increase in the ratcheting strain and reached the tertiary stage later than the uncoated sample at 238 MPa. These results indicate that under the same stress, the Cr-coated sample shows the slowest ratcheting strain accumulation while the TiCrAlN-coated sample shows the fastest accumulation, which can explain the longer fatigue life of the Cr-coated sample and the shorter fatigue life of the TiCrAlN one.

4.3. In-situ observations of deformation and crack evolution

To understand the effect of the coatings on the fatigue life of the Zr-4 substrate, in-situ observations were carried out to reveal the deformation mechanism and crack evolution in different samples. Fig. 8 displays the fatigue deformation features of the uncoated Zr-4 alloy under a maximal stress of 215 MPa. As seen in Fig. 8(a), the equiaxed grains had an average size of approximately 20 μm, and no initial cracks were found in the as-received Zr-4 alloy. After 1500 cycles, slip lines inclined in the loading direction were formed in a few grains owing to soft orientations favorable for prismatic or basal slip deformation, and the concave-convex phenomenon occurred, as shown in Fig. 8(b). As the number of loading cycles increased, plastic deformation accumulated, which aggravated the concave-convex phenomenon, and the slip lines were widely distributed in a majority of the grains (see Fig. 8(c)). Micro-cracks and micro-voids were clearly visible after 19210 cycles (Fig. 8(d)) due to the impingement of slip bands against the grain boundary or intersection between different slip bands [31]. The propagation of micro-cracks and the coalescence with adjacent cracks led to the ultimate fracture of the Zr-4 alloy.

Fig. 9 shows the surface morphology and crack evolution of the TiCrAlN-coated Zr-4 alloy under 215 MPa at 400°C. No initial cracks were observed on the coating surface before the fatigue test (see Fig. 9(a)). However, multiple surface cracks formed after only 20 cycles (see Fig. 9(b)). The cracks were generally parallel to one another and vertical to the loading direction, which is similar to those reported in other brittle ceramic coatings [32]. The early cracks were due to the lower ductility of the ceramic TiCrAlN coating compared to the ductile Zr-4 substrate. As the number of loading cycles increased, new cracks appeared, and the crack density increased (see Fig. 9(c)). In addition, the crack opening displacements became larger as the number of cycles increased, which demonstrates the lower plastic deformability of TiCrAlN coating compared to the Zr-4 substrate. In the late stage of fatigue loading cycles, the cracks initiated and propagated rapidly in the substrate, leading to the ultimate fracture (see Fig. 9(d)). During the fatigue loading cycles, spallation of the TiCrAlN coating did not occur, even after fracture with large macroscopic deformation, which reflects good adhesion of the TiCrAlN coating.

From the results shown in Figs. 5–9, it is evident that the fatigue life of the TiCrAlN-coated sample is an order of magnitude lower than that of the uncoated sample at 215 MPa. The significant decrease in the fatigue life is related to the cracking behavior of the TiCrAlN coating. Because of the brittleness of the TiCrAlN coating, cracks may initiate in the coating early and rapidly propagate throughout the entire coating thickness. Any surface cracks could act as stress risers and contribute to early crack initiation in the substrate from the interface, leading to a shorter fatigue life [18].

Fig. 10 shows the surface crack evolution of the Cr-coated Zr-4 alloy at 250 MPa. No initial cracks appeared on the coating surface before cycling (see Fig. 10(a)). Unlike for the TiCrAlN coating, surface cracks did not appear in the Cr coating until a later period of cycling. The first visible surface crack was found after 9212 cycles (88% of the total life, see Fig. 10(b)), which appeared much later than those in the uncoated sample at 250 MPa (see Fig. 6). As the cyclic loading continued and inelastic deformation accumulated, new micro-cracks began to appear, and then the cracks propagated and coalesced with adjacent cracks to form macro cracks

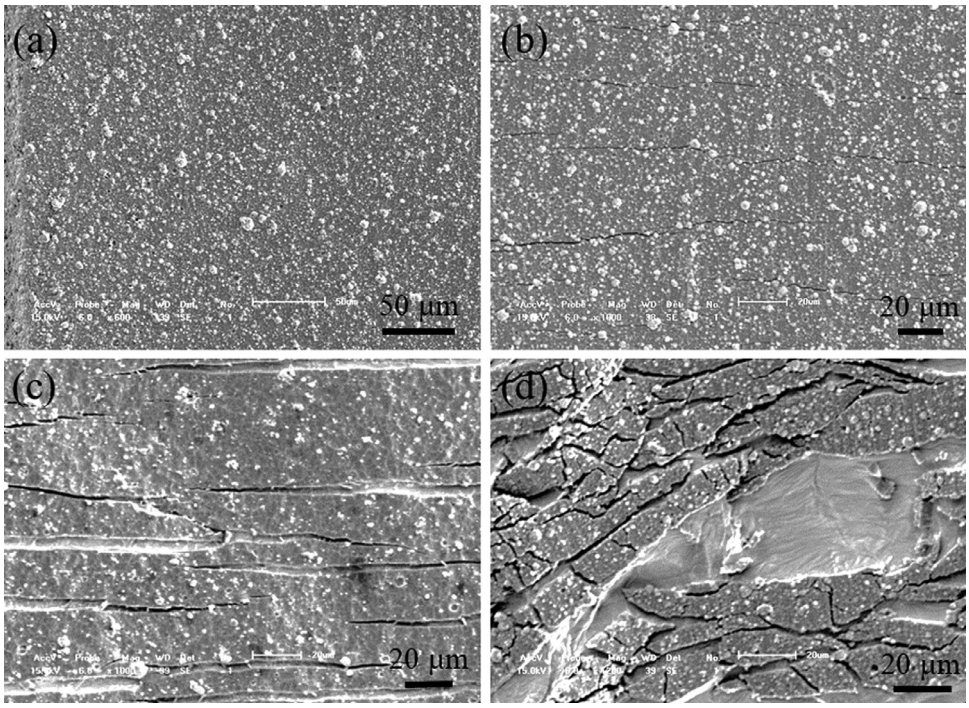

Fig. 9. In-situ observations of the surface crack evolution on the TiCrAlN-coated Zr-4 alloy under 215 MPa at 400°C: (a) 0, (b) 20, (c) 3700, and (d) 5560 cycles.

(see Figs. 10(c)-10(g)). At the end of cycling, crack propagation in the substrate led to the ultimate fracture of the samples, and no coating spallation appeared owing to its good interfacial adhesion (see Figs. 10(h) and 10(i)).

Based on a comparison of Figs. 9 and 10, the surface crack evolution process in the TiCrAlN coating and Cr coating was remarkably different, which led to different mechanisms influencing the fatigue lives. Unlike those in the TiCrAlN ceramic coating, the cracks in the Cr coating were relatively small and separated rather than slender and parallel owing to the crystallography of the Cr coating. In addition, the late time for surface crack initiation under severe plastic deformation reflects the high fracture toughness and ductility of the Cr coating, as well as the suitable compatibility between the Cr coating and the substrate. Because the Cr coating protected the substrate from cracks initiating on its surface, the Cr-coated sample had a longer fatigue life than the uncoated one. In addition, the presence of the Cr coating postponed crack initiation in the substrate from the interface, and thus prolonged the fatigue life of the sample.

4.4. Fractography analysis

A number of uncoated and coated samples were closely examined in an SEM to obtain a general characterization of the fracture surfaces. Fig. 11 shows the fracture surface of the uncoated Zr-4 sample after fatigue testing. Fig. 11(a) shows the overall appearance of the fracture surface, which indicates extreme plastic deformation both on the sample surface and in the interior region. A magnified view of the rectangular region in Fig. 11(a) is shown in Fig. 11(b), in which the sample surface shows a waved morphology, and secondary cracks or pores are evident in the subsurface region. This type of fracture is usually observed in metals exhibiting good ductility and is associated with the deformation mechanism of multiple slips. Fatigue striations were occasionally observed. In addition, micro-voids and secondary cracks were widely found beneath the sample surface, which tend to cause multiple crack initiation sites and facilitate fatigue crack propagation by crack coalescence. Fig. 11(c) shows the instantaneous fracture zone, where exhibits widely distributed dimples and micro-voids due to tensile overload.

Fig. 12 shows the fracture surface of the TiCrAlN-coated sample after fatigue testing. As shown in Fig. 12(a), multiple cracks appeared on the coating surface near the fracture section. The TiCrAlN coating showed no obvious plastic deformation, revealing its brittle fracture property. Nevertheless, the TiCrAlN coating maintained a good bond with the substrate even after fracture. In contrast, remarkable deformation bands were noticeable in the Zr-4 substrate beneath the coating, as seen on the fracture surface in Fig. 12(b), due to the large amount of multiple slip activities. In this case, the fracture of the coating was related to fatigue crack initiation. Fig. 12(c) shows a crack initiation site located at the coating/substrate interface, and the magnified view is shown in Fig. 12(d). The crack initiation and subsequent small crack propagation region appeared relatively flat. Fatigue striations perpendicular to the crack growth direction were commonly observed, which is consistent with those observed in the uncoated Zr-4 sample.

Fig. 13 shows the fracture surface of the Cr-coated sample after fatigue testing. Both the Cr coating and the Zr-4 substrate underwent such extensive plastic deformation that the coating/substrate interface became curved, as shown in Figs. 13(a)-13(c), demonstrating excellent compatibility between the Cr coating and Zr-4 substrate under severe deformation. Slight interfacial delamination was observed, as shown in Figs. 13(b) and 13(c), which formed during the final tensile rupture. Because of the difference in the modulus and ductility between Cr and Zr-4, strain mismatch between the Cr coating and Zr-4 substrate will occur during fatigue loading. The difference will be more significant during the fracture process, arising from the large interfacial shear stress, and should result in interfacial fracture. However, no spallation of the coating occurred. As shown in Fig. 13(c), fatigue cracks tend to initiate at the coating or the Cr/Zr-4 interface. The crack propagation region in Zr-4 substrate showed similar fracture features to that of the TiCrAlN-coated sample in Fig. 12. Dimples were also widely observed in the high ΔK region of the Zr-4 substrate, as shown in Fig. 13(d).

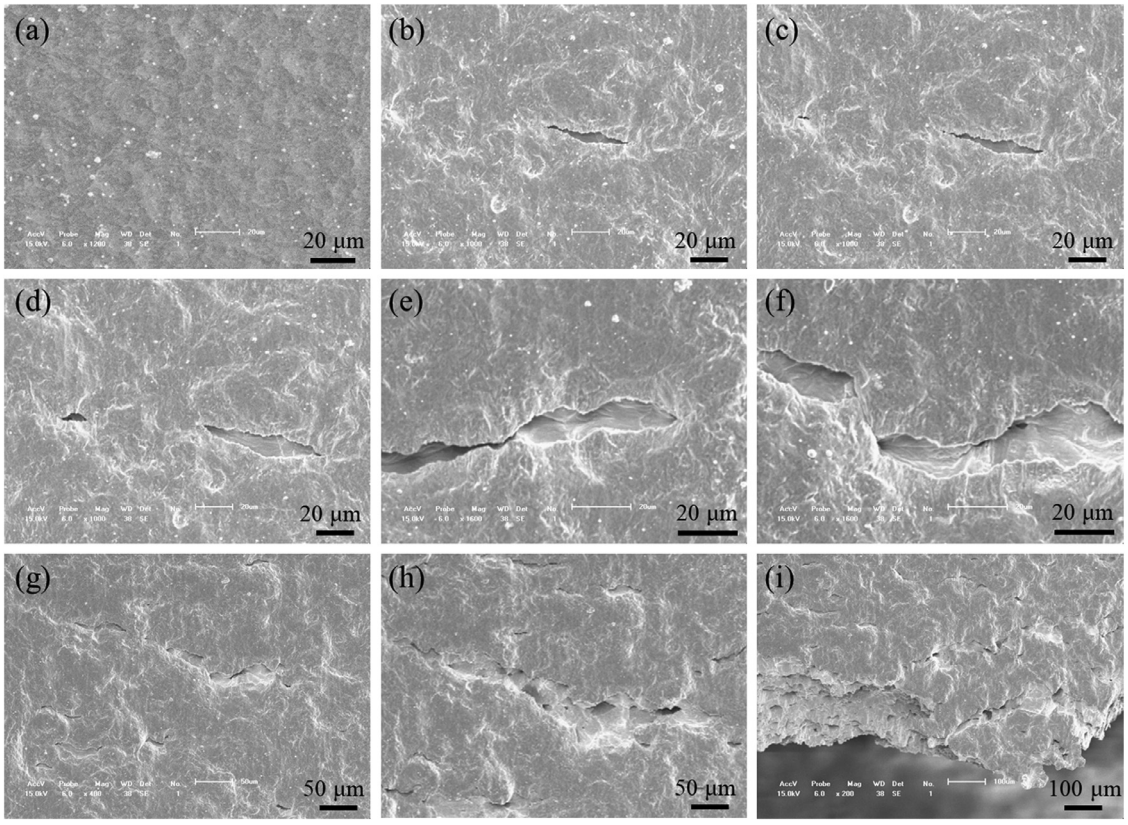

Fig. 10. In-situ observations of the surface crack evolution on the Cr-coated Zr-4 alloy under 250 MPa at 400°C: (a) 0, (b) 9212, (c) 9305, (d) 9725, (e) 9903, (f) 10143, (g) 10232, (h) 10438, and (i) 10440 cycles.

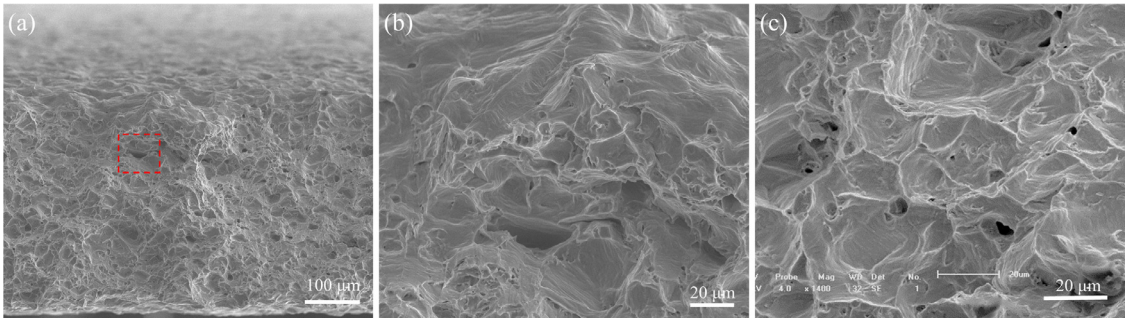

Fig. 11. Fatigue fracture surface of the uncoated Zr-4 alloy after testing: (a) a view under low magnification, (b) a magnified view of the zone marked with red box in (a), and (c) plastic dimples and voids in the instantaneous fracture zone.

4.5. Observation on the longitudinal section

In addition to the fracture surfaces, longitudinal sections parallel to the loading direction were prepared and subjected to SEM observation. Fig. 14 shows the features of a longitudinal section of the TiCrAlN-coated sample near the fracture region after fatigue testing. As shown in Figs. 14(a) and 14(b), multiple vertical cracks were formed in the coating because of its low fracture toughness. No interfacial cracks were found near the vertical crack tips because of the high interfacial adhesion. In the later stage of fatigue cycling, once the accumulated strain reaches a critical value, vertical cracks may continue to penetrate into the Zr-4 substrate, such as those shown in Figs. 14(c) and 14(d). Hence, it was experimentally proved that multiple vertical cracks in the TiCrAlN coating would act as pre-notches, which is the primary mechanism that reduces the fatigue life of the TiCrAlN-coated sample.

The features of a longitudinal section of the Cr-coated sample are presented in Fig. 15, which shows a different fracture mode compared with that of the TiCrAlN-coated sample. In Fig. 15(a), there are fewer cracks in the Cr coating that penetrate into the substrate compared with the TiCrAlN coating, indicating a better fatigue crack resistance of the Cr coating. Fig. 15(b) shows that the coating surface profile appears to fluctuate more than in the as-received condition, suggesting that the Cr coating had undergone severe plastic flow under excessive deformation. Near the fracture region of the sample, a few vertical cracks penetrate slightly into the substrate but no interfacial cracks were found, as shown in Fig. 15(c). It can be seen that the Cr coating exhibited a protective or prohibitive effect on the crack initiation process in the Zr-4 substrate. Because of the excellent deformability of Cr at 400°C, neither the Cr coating nor the Zr-4 substrate exhibited any cracks until approximately 90% of the total fatigue life, as shown in Fig. 10. Figs. 15(a) and 15(c) experimentally verify the excellent fatigue

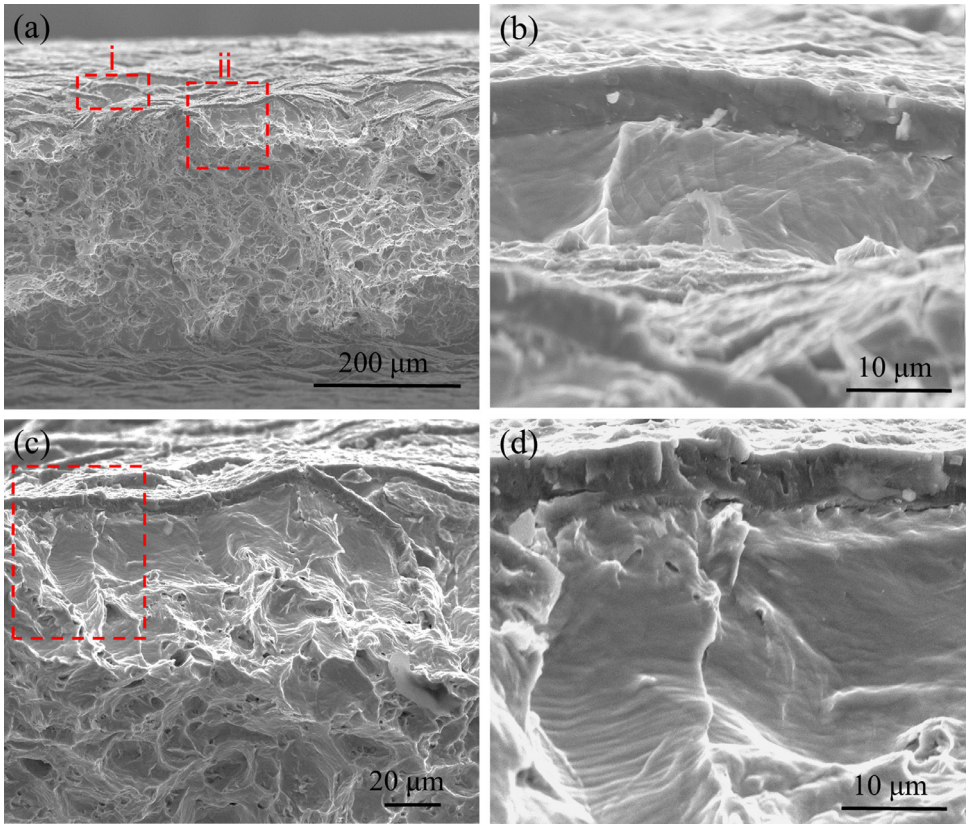

Fig. 12. Fatigue fracture surface of the TiCrAlN-coated Zr-4 alloy after testing: (a) a view under low magnification, (b) a magnified view of area i in (a) showing the surface crack near the fracture surface, (c) a magnified view of area ii in (a) showing the crack initiation and propagation zones, and (d) a view of the crack propagation zone under high magnification.

crack resistance of the Cr coating, unlike that of the TiCrAlN coating (Fig. 14), that is due to the higher fracture toughness of Cr compared with that of TiCrAlN [26]. Hence, both beneficial effects on crack initiation and propagation mentioned above contributed to the enhanced fatigue properties of the Cr-coated sample compared with those of the other two samples.

4.6. Numerical analysis of the stress and cracking in the two coatings

To further understand the stress evolution and vertical cracking in the TiCrAlN and Cr coatings, comparative numerical analyses were carried out. As described in Section 3, uniaxial tensile loads were applied to the FE models to study the accumulation of ratcheting strain during fatigue tests. Fig. 16 shows the FE simulation results of the TiCrAlN- and Cr-coated Zr-4 alloys under different tensile strains ε at 400°C. The in-plane stresses σ_{xx} for both coatings increased with increasing tensile strain in the early stage. After the damage was initiated and accumulated under continuous loading, the stresses in the cohesive elements decreased to zero to form vertical cracks in the coatings. As seen in Figs. 16(a), 16(b), 16(e), and 16(f), at $\varepsilon = 2\%$, vertical cracks formed and penetrated through the thickness of the TiCrAlN coating, while no vertical cracking occurred in the Cr coating. These calculations are consistent with the experimental results that crack initiation occurs earlier in the TiCrAlN coating during the early period of the fatigue test in comparison with the Cr coating. As seen in Fig. 16(e), despite the lack of vertical cracking, damage was already accumulating in the Cr coating. The stress concentration near the interface indicates that vertical cracks may initiate from the interface as the strain increases further. As seen in Figs. 16(c), 16(d), 16(g), and 16(h), at $\varepsilon = 10\%$, the crack opening widened in the TiCrAlN coating, and a vertical crack with a large crack opening finally appeared in the Cr coating. The appearance of vertical cracks led to stress redistribution in the coating systems. Specifically, remarkable out-of-plane stress σ_{yy} and shear stress σ_{xy} formed near the vertical crack tips, which could act as driving forces for the interfacial cracks. However, no interfacial cracks were evident in the experimental results, which is attributed to the good interfacial adhesion properties for both the TiCrAlN and Cr coating. Based on the numerical analyses, vertical crack initiation is closely related to the mechanical and fracture properties of the coatings. Again, the early crack initiation and high crack density in the brittle TiCrAlN coating is attributed to its low fracture toughness, while the late crack initiation and low crack density in the ductile Cr coating is attributed to its high fracture toughness and good plastic deformability.

Based on the experimental and numerical results in this study, the fatigue lives of the coated samples are closely related with the cracking behavior of the coating. A schematic is shown in Fig. 17 that summarizes the distinct fracture modes of the two coated samples. In Fig. 17(a), penetrating vertical cracks with a high crack density are generated in the brittle TiCrAlN coating in the early period of fatigue cycling due to its low ductility and toughness. The vertical cracks in the coating will cause stress concentrations around the crack tips near the Zr-4 substrate, promoting crack propagation into the substrate as the number of fatigue cycles increases. The earlier failure of the TiCrAlN coating leads to a short fatigue life for the TiCrAlN-coated sample. Furthermore, the thickness of the TiCrAlN coating may also affect the cracking behavior and fatigue life of the sample. Based on the shear-lag model for predicting the cracking behavior of ceramic coatings, a thicker coating leads to a lower crack density, i.e. less numbers of surface cracks [33]. As the ceramic TiCrAlN coating becomes thicken,

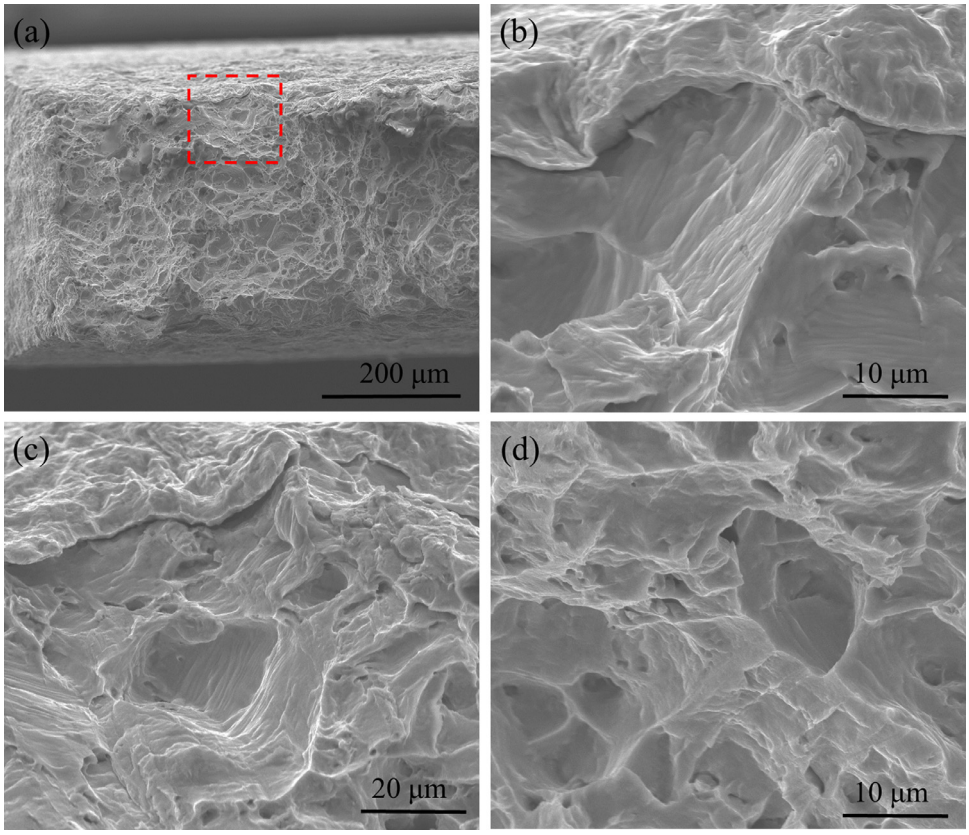

Fig. 13. Fatigue fracture surface of the Cr-coated Zr-4 alloy after testing: (a) a view under low magnification, (b) a view of the rough interface between the coating and the substrate under high magnification, (c) a magnified view of the crack initiation and propagation zones marked with a red box in (a), and (d) plastic dimples and voids in the instantaneous fracture zone.

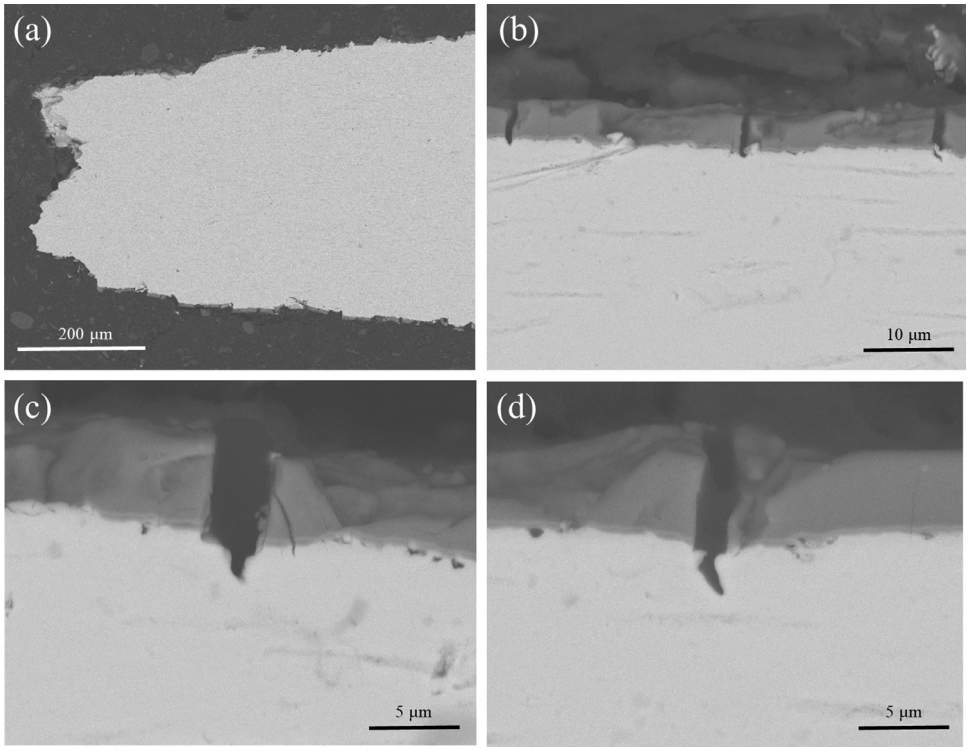

Fig. 14. Features of a longitudinal section of the TiCrAlN-coated Zr-4 alloy parallel to the loading direction after the fatigue test: (a) overview of the longitudinal section near the fracture region, (b) vertical cracks in the coating, (c) a vertical crack that penetrated into the Zr-4 substrate, and (d) another crack that penetrated into the Zr-4 substrate.

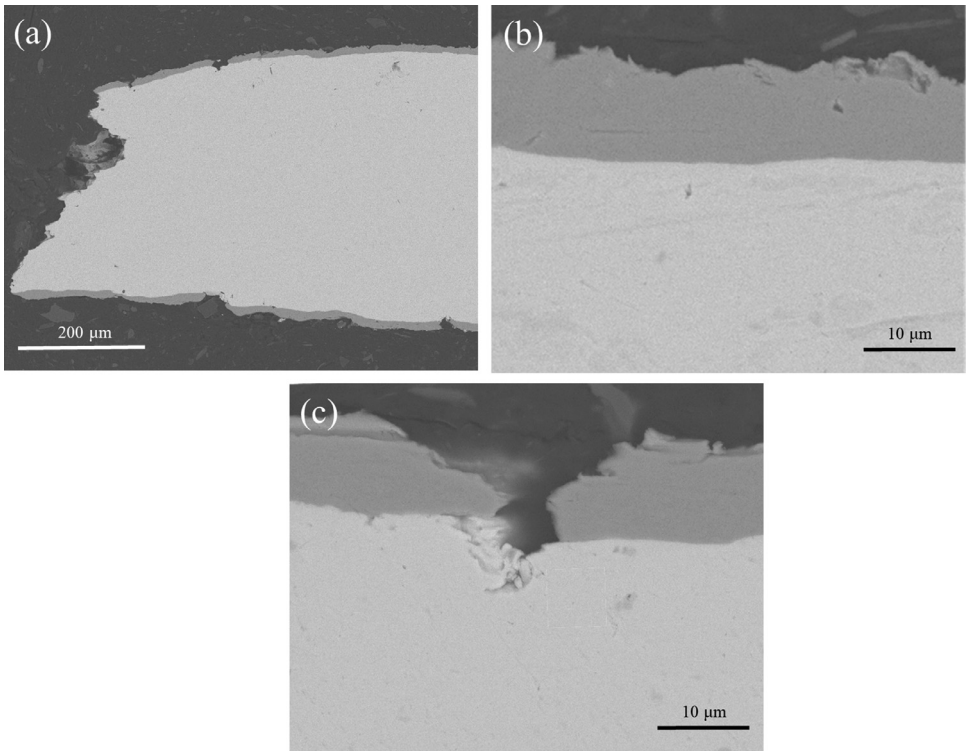

Fig. 15. Features of a longitudinal section of the Cr-coated Zr-4 alloy after testing: (a) an overview of the longitudinal section near the fracture surface, (b) the rough surface of the coating, and (c) vertical cracks that propagated into the Zr-4 substrate.

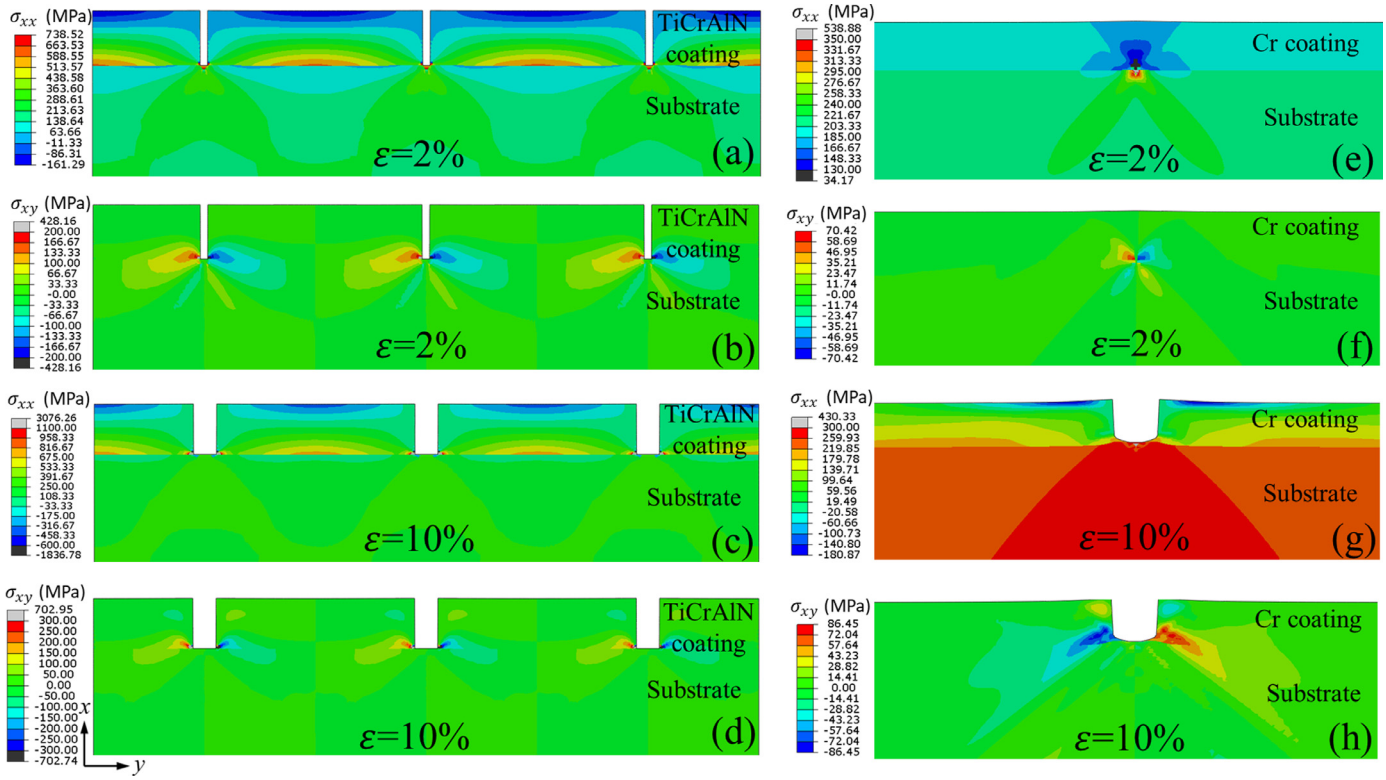

Fig. 16. Finite element simulation results of the TiCrAlN- and Cr-coated Zr-4 alloys under different tensile strains ε at 400°C: (a) σ_{xx} in TiCrAlN-coated Zr-4 with $\varepsilon = 2\%$, (b) σ_{xy} in TiCrAlN-coated Zr-4 with $\varepsilon = 2\%$, (c) σ_{xx} in TiCrAlN-coated Zr-4 with $\varepsilon = 10\%$, (d) σ_{xy} in TiCrAlN-coated Zr-4 with $\varepsilon = 10\%$, (e) σ_{xx} in Cr-coated Zr-4 with $\varepsilon = 2\%$, (f) σ_{xy} in Cr-coated Zr-4 with $\varepsilon = 2\%$, (g) σ_{xx} in Cr-coated Zr-4 alloy $\varepsilon = 10\%$, and (h) σ_{xy} in Cr-coated Zr-4 with $\varepsilon = 10\%$.

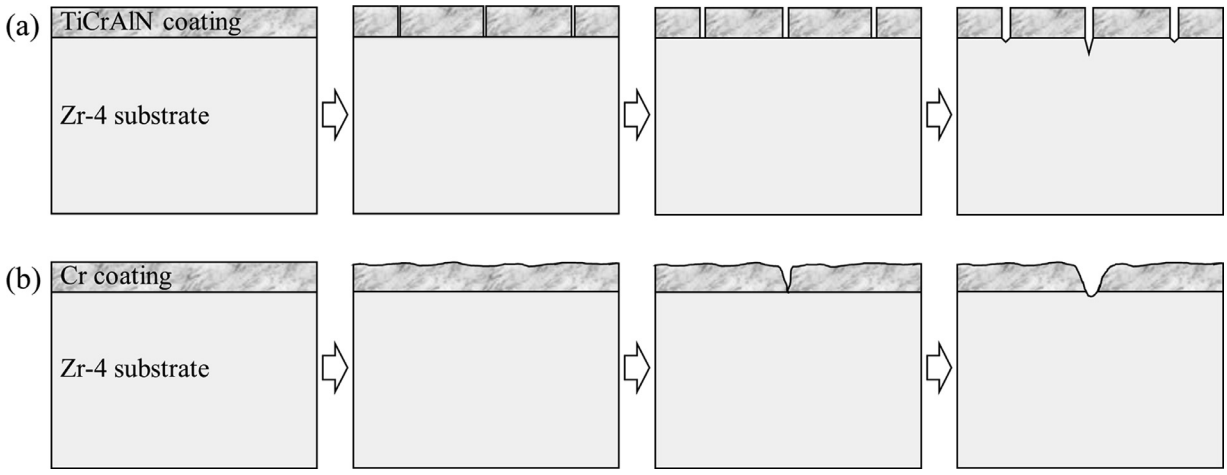

Fig. 17. Schematic of the fatigue fracture behaviors in the coated Zr-4 alloys at 400°C: (a) TiCrAlN-coated sample and (b) Cr-coated sample.

the surface crack density will decrease under fatigue loadings, thus there will be less "pre-notches" for the substrate and the fatigue life of the coated sample will be longer. However, no matter how thick the TiCrAlN coatings is, the fatigue life of the coated sample is shorter than that of the uncoated sample. In Fig. 17(b), because of its high fracture toughness and ductility, the Cr coating is free from cracks during a long period of cycling. In the process of plastic deformation during cycling, the Cr coating could prevent the dislocations escaping from the crystal surface of the substrate. Under the effect of the Cr coating, although dislocations could pile-up at the surface of the substrate, the sliding deformation of the materials was inhibited [19]. In the late stage, driven by the large cyclic plastic deformation, a vertical crack is initiated in the coating, which is followed by the crack penetrating the substrate. Crack initiation in the substrate is postponed owing to the protection of the Cr coating. Furthermore, the residual stress after coating might also affect the fatigue life of the coated sample. As reported in Refs. [17,18], the compressive residual stresses in the thin coatings developed during the deposition processes played positive roles in inhibiting fatigue crack initiation and prolonging the fatigue lives of the coated samples. As reported in our previous work [24], the residual stress in the Cr coating examined by a XRD 2θ-$\sin^2\Psi$ method was -305 MPa. Apart from the remarkable plastic deformation capability in the Cr coating, the compressive residual stress may be another key factor to improve the fatigue life. It should be emphasized that different ATF coatings may play different roles in altering the fatigue properties of a coated alloy. Therefore, it is critical to investigate the mechanical strength and understand the deformation and failure mechanism of the coated alloys in the screening and evaluation of ATF coating candidates.

5. Conclusions

The effects of two accident tolerant coatings, i.e., a Cr coating and a TiCrAlN coating, on the fatigue behavior of the Zr-4 alloy at 400°C were studied by an in-situ SEM technique. Note that the testing was performed in vacuum and additional work is needed to determine if trends remain the same in light water reactor environments. The following conclusions were obtained:

(1) Fatigue test results showed that the Cr coating evidently improved the fatigue life of the Zr-4 alloy while the TiCrAlN coating decreased the fatigue life of Zr-4 alloy remarkably.

(2) Because of the average stress effect, all samples showed ratcheting strain during cyclic loading, with the magnitude of the ratcheting strain in the following order: Cr-coated < uncoated < TiCrAlN-coated Zr-4. The ratcheting strain rationalized the fatigue life variation of the uncoated and coated Zr-4 samples in this study.

(3) In-situ SEM observations revealed that the Cr coating exhibited good plastic deformability with the Zr-4 substrate until the late stage of fatigue life. In contrast, for the TiCrAlN coating, multiple cracks formed in the early stage of fatigue life. The distinct effects of different coatings were confirmed by analysis of the fracture surfaces and longitudinal sections of the fatigue samples. Hence, fatigue life variation in the coated Zr-4 samples can be attributed to the deformation and cracking behavior of the coatings under cyclic loading.

(4) Fractography analysis indicated significant plastic deformation in the uncoated Zr-4 alloy, in which the voids and microcracks formed by slip impingements were responsible for the facture. For the TiCrAlN-coated sample, multiple cracks in the coating showed brittle cleavage features, which acted as crack initiation sites to promote crack propagation into the substrate. For the Cr-coated sample, the Cr coating showed remarkable plastic deformation associated with the Zr-4 substrate. Striations were commonly observed in the stable crack propagation region of the Zr-4 alloy. No spallation of either the Cr or TiCrAlN coating was observed, indicating satisfactory bonding strengths of the ATF coatings in this study.

(5) Finite element simulations based on the cohesive element method indicated that the pre-failure of the brittle TiCrAlN coating with its low fracture toughness promoted early crack initiation in the Zr-4 substrate, leading to a short fatigue life. For the Cr coating with its high fracture toughness and good ductility, crack initiation in the substrate was postponed, leading to a longer fatigue life for the Cr-coated sample.

Declaration of Competing Interest

The authors declare that they have no known competing financial interests or personal relationships that could have appeared to influence the work reported in this paper.

CRediT authorship contribution statement

Xianfeng Ma: Writing - original draft, Writing - review & editing, Conceptualization, Funding acquisition. **Hailin Zhai:** Investigation, Formal analysis. **Fanqiang Meng:** Formal analysis. **Jishen Jiang:** Methodology, Data curation, Supervision, Software, Writing - original draft, Writing - review & editing. **Xiujie He:** Formal analysis. **Yanying Hu:** Investigation. **Wenjie Zhang:** Validation. **Jiajun**

Tu: Visualization. **Donghui Wei:** Data curation. **Biao Wang:** Conceptualization, Supervision.

Acknowledgements

This project is supported by the National Natural Science Foundation of China (No. 52005523, 11902370, U2032143), Guangdong Major Project of Basic and Applied Basic Research (2019B030302011), International Sci & Tech Cooperation Program of GuangDong Province (2019A050510022), Key-Area Research and Development Program of GuangDong Province (2019B010943001, 2017B020235001), China Postdoctoral Science Foundation (2019M653173 and 2019TQ0374), Guangdong Education Department Fund (2016KQNCX005), and Fundamental Research Funds for the Central Universities (19lgpy304).

References

[1] R. Krishnan, M.K. Asundi, Zirconium alloys in nuclear technology, P. Indian A. S. 4 (1) (1981) 41–56.
[2] S.J. Zinkle, K.A. Terrani, J.C. Gehin, et al., Accident tolerant fuels for LWRs: A perspective, J. Nucl. Mater. 448 (1-3) (2014) 374–379.
[3] C. Tang, M. Stueber, H.J. Seifert, et al., Protective coatings on zirconium-based alloys as accident-tolerant fuel (ATF) claddings, Corros. Rev. 35 (3) (2017) 141–165.
[4] B.R. Maier, B.L. Garcia-Diaz, B. Hauch, et al., Cold spray deposition of Ti2AlC coatings for improved nuclear fuel cladding, J. Nucl. Mater. 466 (2015) 712–717.
[5] J.H. Chun, S.W. Lim, B.D. Chung, et al., Safety evaluation of accident-tolerant FCM fueled core with SiC-coated zircalloy cladding for design-basis-accidents and beyond DBAs, Nuc. Eng. Des. 289 (2015) 287–295.
[6] Y. Katoh, G. Vasudevamurthy, T. Nozawa, et al., Properties of zirconium carbide for nuclear fuel applications, J. Nucl. Mater. 441 (1-3) (2013) 718–742.
[7] X.F. Ma, Y.W. Wu, J. Tan, et al., Evaluation of corrosion and oxidation behaviors of TiAlCrN coatings for nuclear fuel cladding, Surf. Coat. Tech. 358 (2019) 521–530.
[8] J.H. Park, H.G. Kim, J. Park, et al., High temperature steam-oxidation behavior of arc ion plated Cr coatings for accident tolerant fuel claddings, Surf. Coat. Tech. 280 (2015) 256–259.
[9] S. Hao, L. Zhao, D. He, Surface microstructure and high temperature corrosion resistance of arc-sprayed FeCrAl coating irradiated by high current pulsed electron beam, Nuclear Instruments and Methods in Physics Research Section B: Beam Interactions with Materials and Atoms 312 (2013) 97–103.
[10] Kuprin A.S., Belous V.A., V.N. Voyevodin, et al., Vacuum-arc chromium-based coatings for protection of zirconium alloys from the high-temperature oxidation in air, J. Nucl.Mater. 465 (2015) 400–406.
[11] Y. Wang, H. Tang, X. Han, et al., Oxidation resistance improvement of Zr-4 alloy in 1000°C steam environment using ZrO2/FeCrAl bilayer coating, Surf. Coat. Tech. 349 (2018) 807–815.
[12] E. Alat, A.T. Motta, R.J. Comstock, et al., Multilayer (TiN, TiAlN) ceramic coatings for nuclear fuel cladding. J. Nucl. Mater. 478 (2016) 236–244.
[13] H.G. Kim, I.H. Kim, Y.I. Jung, et al., Adhesion property and high-temperature oxidation behavior of Cr-coated Zircaloy-4 cladding tube prepared by 3D laser coating, J. Nucl. Mater. 465 (2015) 531–539.
[14] J.C. Brachet, I. Idarraga-Trujillo, M. Le Flem, et al., Early studies on Cr-Coated Zircaloy-4 as enhanced accident tolerant nuclear fuel claddings for light water reactors, J. Nucl. Mater. 517 (2019) 268–285.
[15] M. Wen, H. Li, D. Yu, et al., Uniaxial ratcheting behavior of Zircaloy-4 tubes at room temperature, Mater. Design 46 (2013) 426–434.
[16] R. Mušálek, O. Kovářík, T. Skiba, et al., Fatigue properties of Fe–Al intermetallic coatings prepared by plasma spraying, Intermetallics 18 (7) (2010) 1415–1418.
[17] B. Lonyuk, I. Apachitei, J.. Duszczyk, Effect of high-phosphorus electroless nickel coating on fatigue life of Al–Cu–Mg–Fe–Ni alloy, Scripta Mater 57 (8) (2007) 783–786.
[18] B. Lonyuk, I. Apachitei, J.. Duszczyk, The effect of oxide coatings on fatigue properties of 7475-T6 aluminium alloy, Surf. Coat. Tech. 201 (21) (2007) 8688–8694.
[19] Y. Bai, Y. Xi, K. Gao, et al., Brittle coating effects on fatigue cracks behavior in Ti alloys, Int. J. Fatigue 125 (AUG.) (2019) 432–439.
[20] M.Y.P Costa, M.L.R Venditti, H.J.C Voorwald, et al., Effect of WC–10% Co–4% Cr coating on the Ti–6Al–4V alloy fatigue strength, Mater. Sci. Eng. A 507 (1-2) (2009) 29–36.
[21] J. Jiang, W. Wang, X. Zhao, et al., Numerical analyses of the residual stress and top coat cracking behavior in thermal barrier coatings under cyclic thermal loading, Eng. Fract. Mech. 196 (2018) 191–205.
[22] H. Cheng, G. Chen, Z. Zhang, et al., Uniaxial ratcheting behaviors of Zircaloy-4 tubes at 400°C, J. Nucl. Mater. 458 (2015) 129–137.
[23] U. Holzwarth, H. Stamm, Mechanical and thermomechanical properties of commercially pure chromium and chromium alloys, J. Nucl. Mater. 300 (2-3) (2002) 161–177.
[24] J.S. Jiang, H.L. Zhai, P.F. Gong, W.J. Zhang, X.J. He, X.F. Ma, B. Wang, In-situ study on the tensile behavior of Cr-coated zircaloy for accident tolerant fuel claddings, Surf. Coat. Tech. 394 (2020) 125747.
[25] W. Zhu, L. Yang, W.J. Guo, Y.C. Zhou, C. Lu, Determination of interfacial adhesion energies of thermal barrier coatings by compression test combined with a cohesive zone finite element model, Int. J. Plasticity 64 (2015) 76–87.
[26] K. Hong, J.R. Barber, M.D. Thouless, W. Lu, Cracking of Cr-coated accident-tolerant fuel during normal operation and under power-ramping conditions, Nucl. Eng. Des. 353 (2019) 110275.
[27] S. PalDey, S.C. Deevi, Properties of single layer and gradient (Ti, Al) N coatings, Mater. Sci. Eng. A 361 (1-2) (2003) 1–8.
[28] X. He, Z. Tian, B. Shi, et al., Effect of gas pressure and bias potential on oxidation resistance of Cr coatings, Ann. Nucl. Energy 132 (2019) 243–248.
[29] G. Hong, C.. Xu, Effect of axial ratcheting deformation on torsional low cycle fatigue life of lead-free solder Sn–3.5Ag, Int. J. Fatigue 31 (2) (2009) 276–283.
[30] R.S. Rajpurohit, N.C.S. Srinivas, S.R. Singh, et al., Fatigue behavior of Zircaloy-2 under asymmetric loading at 400°C, Int. J. Pres. Ves. Pip. 159 (2018) 84–92.
[31] Z.F. Zhang, Z.G. Wang, Dependence of intergranular fatigue cracking on the interactions of persistent slip bands with grain boundaries, Acta Mater 51 (2) (2003) 347–364.
[32] M. Zhou, W.B. Yao, X.S. Yang, et al., In-situ and real-time tests on the damage evolution and fracture of thermal barrier coatings under tension: A coupled acoustic emission and digital image correlation method, Surf. Coat. Tech. 240 (2014) 40–47.
[33] A.P. McGuigan, G.A.D Briggs, V.M. Burlakov, M. Yanaka, Y. Tsukahara, An elastic–plastic shear lag model for fracture of layered coatings, Thin Solid Films 424 (2) (2003) 219–223.